An Experimental Study of the Unsteady Nature of the Viscous Sublayer

L. PHILIP REISS and THOMAS J. HANRATTY

University of Illinois, Urbana, Illinois

Measurements of the fluctuations in the mass transfer rate to small circular electrodes mounted flush with a pipe wall are used to study the unsteady nature of the viscous sublayer. These fluctuations in the mass transfer rate reflect flow fluctuations at $y^+ < ca$ 0.5. From these measurements it is concluded that the flow disturbances are elongated in the direction of flow and are characterized by a time scale equal to the diameter of the pipe divided by the bulk average velocity. An attempt is made to relate the mass transfer fluctuations to the fluctuation in velocity gradient at the wall. It is concluded that the ratio of the root-mean-square fluctuating velocity gradient at the wall to the average velocity gradient at the wall is at least 0.11.

In a previous paper (*13*) a technique for measuring instantaneous rates of mass transfer with a diffusion controlled electrolytic reaction is described. The instantaneous diffusion limited current is measured for the electrochemical reaction

$$Fe(CN)_6^{-3} + e^- \rightarrow Fe(CN)_6^{-4}$$

on a small circular nickel electrode which is mounted flush with a plastic pipe wall. The mass transfer rate is calculated from the measured current with Faraday's law. Measurements which can be made with this technique include the average and the root-mean-square of the fluctuating mass transfer coefficient, frequency spectra of the mean square of the fluctuations in the mass transfer coefficient, and correlations of the simultaneous fluctuations in the mass transfer coefficients from two electrodes spaced at varying intervals both longitudinally and circumferentially.

It was shown in the earlier paper (*13*) that the region of the flow field which influences the mass transfer measurements is of the order of one-tenth the viscous sublayer thickness ($y^+ < 0.5$). Consequently these mass transfer experiments are a possible means for studying the nature of the unsteady flow in the viscous sublayer. This paper describes the results of such a study made in a 1 in. diameter circular pipe. From the fluctuating mass transfer data certain conclusions are drawn regarding the unsteady flow field causing these fluctuations. An attempt is also made to calculate from the mass transfer measurements the magnitude of the flow fluctuations in the immediate vicinity of the wall.

Under the proper circumstances the fluctuations in the mass transfer coefficient can be used to evaluate the local fluctuating velocity gradient at the electrode surface in an analogous way that hot wire anemometer measurements can be used to evaluate velocity fluctuations. In constant current hot wire anemometry the wire current is held constant, and variations in the rate of heat transfer or wire temperature caused by local flow variations are measured as variations in the wire resistance or voltage drop. In the present work the concentration at the electrode surface is constant and essentially equal to zero when the electrolytic reaction is diffusion controlled. Variations in the mass transfer rate caused by local variations in the velocity gradient are measured as variations in the electrode circuit current.

Several limitations of both systems are also similar. The ability of the hot wire anemometer to measure directly high frequency velocity fluctuations is limited by the thermal inertia of the wire. A capacitance effect of the concentration boundary layer over a diffusion controlled electrode limits direct measurement of the high frequency velocity gradient fluctuations. Large turbulent intensities can cause nonlinear response in both systems. Nonuniform flow over the wire length and over the electrode surface can also be a source of error

EXPERIMENTAL

A description of the experimental technique and equipment has already been presented (*13*). The electrolytic reaction was carried out on small circular nickel electrodes made from three wire sizes 14, 22, and 26 B and S gauge. These wires were inserted through the wall near the downstream end of a 1 in. I.D. plastic pipe and glued into place. The electrodes were arranged in the configuration shown in Figure 1 so that longitudinal and circumferential correlations could be measured.

The process of smoothing the protruding wires flush with the pipe wall consisted of hand sanding with progressively finer grades of emery paper and finally buffing with a powered spindle which was covered with soft cloth. The surface roughness of the inside of the plastic pipe over the electrodes was measured with a profilometer and was found to be an order of magnitude smaller than the concentration boundary-layer thickness.

In order to attain good reproducibility of the measurements the following treatment was given the electrodes prior to running. The electrodes were buffed with the power driven spindle and then treated cathodically at −1.5 v. for 10 to 20 min. with 5% sodium hydroxide as an electrolyte. After the test section was rinsed with demineralized water it was installed in the flow system. At the conclusion of a run the test section was disconnected from the flow system, rinsed with demineralized water, and wiped dry with a clean soft cloth. When this procedure was followed the reproducibility of the measurements ranged from 5 to 10%.

Several initial experiments indicated that the electrolytic reaction was diffusion controlled. First the measured limiting current is directly proportional to the bulk composition of ferricyanide in the concentration range from 0.001 to 0.1 molar. Secondly the transference number for a typical electrolyte, 0.01 molar potassium ferricyanide, 0.01 molar potassium ferrocyanide, and 2.1 molar sodium hydroxide, is 0.0018; consequently ionic migration may be neglected. Thirdly there is no difference in frequency spectra measurements made at different applied electrode potentials. Since the reaction rate varies exponentially with the potential, these spectra measurements indicate that the electrode surface reaction kinetics are not influencing the high frequency components of the fluctuations of the mass transfer measurements.

MASS TRANSFER MEASUREMENTS

The three different sized electrodes used represent approximately a four-fold variation in diameter from 0.0398 to 0.1636 cm. The Reynolds number varied from 100 to 35,000 for average measurements and from 2,640 to 35,000 for fluctuation measurements. The electrolyte composition was maintained nearly constant. Slight variations were due to the amount of water used to make up different electrolytes. The

L. Philip Reiss is with the Shell Development Company, Everyville, California.

electrolyte properties varied within the limits shown in Table 1.

The time average mass transfer coefficient $\overline{K}$ for the three different electrode sizes as a function of Reynolds number is shown in Figure 2. The two regimes of flow and the laminar-turbulent transition at a Reynolds number of 2,100 are clearly indicated. The average mass transfer coefficient increases with decreasing electrode size.

The measured mass transfer intensities, defined as the ratio of the root-mean-square of the fluctuating mass transfer coefficient to the time average mass transfer coefficient $\sqrt{\overline{k^2}/\overline{K}}$, are plotted in Figure 3. The intensities are dependent on electrode size. This size effect is due primarily to nonuniform flow over the electrode surface.

Uniform flow over the electrode implies that the size of the electrode is much smaller than the scales of turbulence close to the wall, so that at any instant the velocity over every segment of the electrode is the same. For the experimental system used it was found that the integral scale determined from the longitudinal mass transfer correlations was an order of magnitude larger than the electrode diameters, but the integral scale estimated from the circumferential mass transfer correlations was of the same order as the electrode diameters (see Figures 4 and 5). Consequently the flow appeared to be nonuniform only in the direction normal to the average flow.

For a given flow condition the nonuniformity of the flow increases as the electrode size increases as indicated in Figure 5, where the circular electrodes are shown in scale with the abscissa. The measured mass transfer intensity is lower as the degree of nonuniformity is increased. The measured mass transfer intensity would decrease with increasing electrode size to the point where a very large electrode would average out all the effects of the flow disturbances so that the intensity would be zero.

A correction for nonuniform flow over the length of the wire of a hot wire anemometer has been developed by Skramstad (*4, 7*). It has been shown (*12*) that an analogous procedure can be used to estimate a correction for mass transfer intensities for nonuniform flow if the circular electrode is considered to be a square of equal area. This correction also involves the assumption that the circumferential correlation coefficient varies exponentially with electrode spacing. The limited circumferential correlation data are insufficient to confirm this assumption. However the best fit exponential curve is drawn through the data. On the basis of this arbitrary fit for the circumferential correlation a scale of $\Lambda_c/d = 0.0445$ is obtained. In order to illustrate the effect of nonuniform flow a correction was applied to the intensity data measured at different electrode sizes with a value of $\Lambda_c/d = 0.0445/2$. The effect of this correction, shown in Figure 3, is to bring the data from different sized electrodes into better agreement. The corrected data are greater than the measured data. It appears that the mass transfer intensity measurements made on the smallest electrode, 26 gauge, are not greatly affected by nonuniform flow. It should be emphasized that this correction is being used only to indicate the effect of nonuniform flow on mass transfer intensity measurements. The correction is an approximation because of the arbitrary assumptions involved in its derivation, that is idealized electrode geometry and the arbitrary choice of the variation of circumferential correlation with electrode spacing. The correction was not extended to correlation or spectrum measurements. Consequently only the correlation and spectrum measurements made on the smallest size electrode which is least influenced by nonuniform flow are presented.

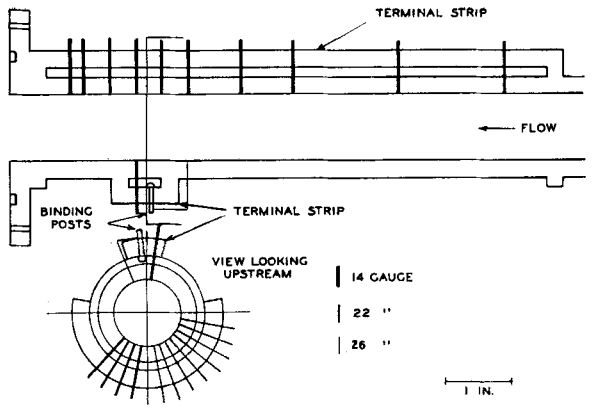

Fig. 1. Diagram of test electrode configuration.

The longitudinal and circumferential mass transfer correlations shown in Figures 4 and 5 were measured on the 26 gauge electrodes at three different Reynolds numbers. The electrode spacing is made dimensionless by the use of the tube diameter. Over this very limited range of Reynolds numbers there is no large variation of the longitudinal integral scale which was calculated with graphical integration. This integral scale is of the order of the pipe radius, while the circumferential integral scale estimated from the arbitrary exponential curve through the limited data is an order of magnitude smaller than the pipe radius.

The frequency spectra measured at different Reynolds numbers on a 26 gauge electrode are shown in Figure 6. The frequency is made dimensionless with a time scale which is the ratio of the pipe diameter to the bulk averaged velocity. The dimensionless spectral density function becomes

$$\frac{W_k U_{av}}{\overline{k^2} d} \qquad (1)$$

There is a remarkable degree of similarity at high frequencies among the spectra measured at different Reynolds numbers. The dissimilarity at low frequencies might be due to the difficulties encountered in making accurate low frequency measurements with the present experimental equipment. It is interesting to note that the fluctuating mass transfer process at the pipe wall appears to be dependent on a time scale which is based on bulk parameters. The use of a time scale defined in terms parameters of the wall region ν/u^{*2} was not successful (*12*) in correlating the spectra.

A comparison of mass transfer spectra with velocity spectra measured with the hot wire anemometer in the viscous sublayer region of a pipe (*14*), channel (9), and boundary layer (8), and pressure spectra, measured with a pressure transducer which is mounted

Table 1. Variation in Electrolyte Properties

Ferrocyanide concentration	0.0111	-	0.0122	molar
Ferricyanide concentration	0.00977	-	0.01069	molar
Sodium hydroxide concentration	2.14	-	2.23	molar
Density	1.090	-	1.096	g./cc.
Viscosity	1.418	-	1.448	centipoise
Diffusion coefficient	5.11×10^{-6}	-	5.22×10^{-6}	sq. cm./sec.
Schmidt number	2,510	-	2,610	

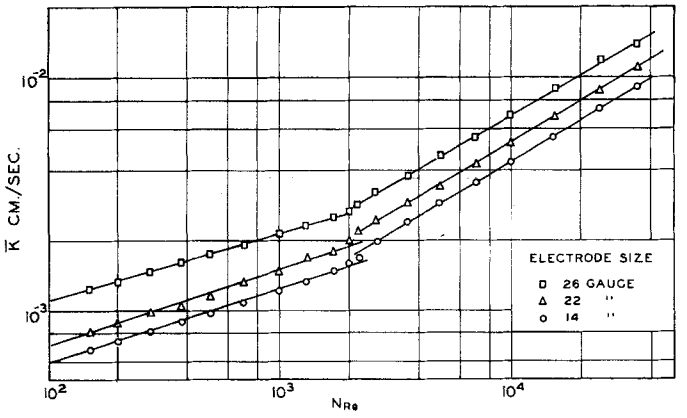

Fig. 2. Average mass transfer coefficient.

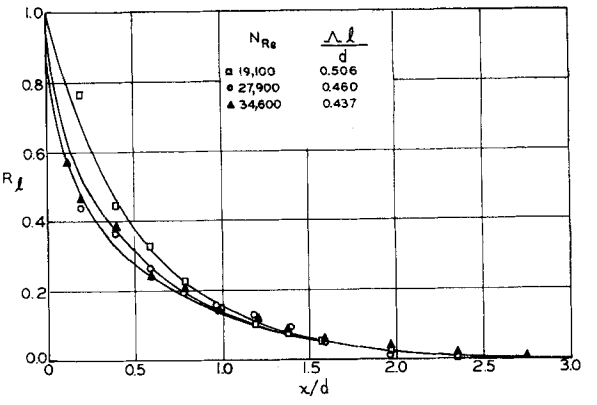

Fig. 4. Longitudinal correlation.

on the wall of a wind tunnel (6), has been made in Figure 7 with the time scale based on bulk parameters. The characteristic lengths used to define the time scale are the radius, half-width, and displacement thickness for the pipe, channel, and boundary layer respectively. The velocities used are the bulk average velocity for the pipe and channel and the free stream velocity for the boundary layer. When this time scale, which differs from Figure 6 by a factor of 2 is used, the dimensionless spectral density functions for velocity pressure and mass transfer become

$$\frac{W_u U_{av}}{\overline{u^2}\, a} \quad \text{velocity} \qquad (2)$$

$$\frac{W_p U_{av}}{\overline{p^2}\, a} \quad \text{pressure} \qquad (3)$$

$$\frac{W_k U_{av}}{\overline{k^2}\, a} \quad \text{mass transfer} \qquad (4)$$

RELATION OF MASS TRANSFER MEASUREMENTS TO THE VELOCITY FIELD NEAR THE WALL

The mass transfer measurements can be related to the fluctuating velocity field near the electrode if the following assumptions are valid.

1. The scales of turbulence are large with respect to the electrode diameter so that the flow is uniform over the electrode surface.

2. The concentration boundary-layer thickness is smaller than the viscous sublayer thickness, and both regions are small compared with the pipe diameter.

3. The local relative turbulent intensities in the x and z directions are small.

4. The fluid properties density, viscosity, and diffusion coefficient are constant.

The effect of nonuniform flow has already been discussed, and it was concluded that none of the electrodes were completely satisfactory but that the smallest electrode is least affected by nonuniform flow. Thus the present analysis will be applied only to data measured on the 26 gauge electrode.

The average concentration boundary layer thickness may be approximated by the Nernst diffusion-layer concept (3)

$$\delta_c = \frac{D}{\bar{K}} \qquad (5)$$

The viscous sublayer thickness is defined as the point where the average velocity data deviate from a linear variation with distance from the wall. This occurs at $y^+ = 5$, and the viscous sublayer thickness is given by

$$\delta_v = \frac{5\nu}{u^*} \qquad (6)$$

Figure 8 shows the variation of δ_c/δ_v and δ_v/d with Reynolds number. For the whole range of Reynolds numbers δ_c is less than one-tenth of δ_v and δ_v is much smaller than the pipe diameter so that the curvature of the pipe may be neglected.

The assumption of small $\sqrt{\overline{u^2}/U}$ appears valid as the largest value of the velocity intensity calculated directly from mass transfer intensities is 0.11. The second-order terms would be approximately an order of magnitude smaller than the first-order tems.

The temperature of the electrolyte was carefully controlled at a constant value of 25°C. Therefore the variation of density, viscosity, and diffusion coefficient due to temperature variations is eliminated. The variation of density and viscosity due to variations in ferrocyanide-ferricyanide concentration is also negligible because of the very dilute solutions (0.01 molar) of ferrocyanide-ferricyanide used.

The direction l is defined as the direction of flow at any instant such that flow in the m direction is always zero. The direction of average flow is designated as x, while the direction normal to average flow is z. The direction outward from the wall is y. The instan-

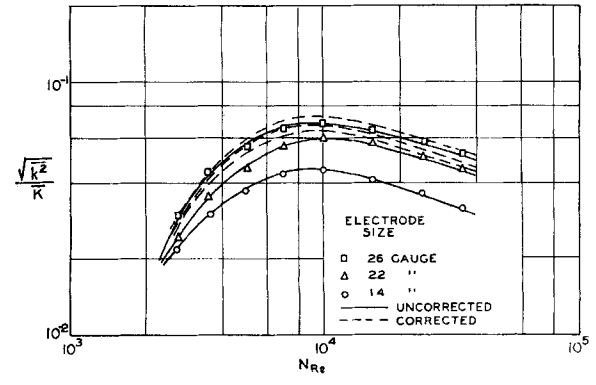

Fig. 3. Mass transfer intensity.

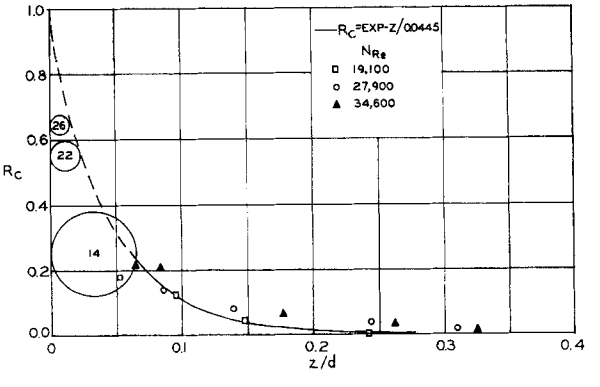

Fig. 5. Circumferential correlation.

taneous mass balance of ferricyanide may be written as

$$\frac{\partial C}{\partial t} + v\frac{\partial C}{\partial y} + U_l\frac{\partial C}{\partial l} = D\left(\frac{\partial^2 C}{\partial y^2} + \frac{\partial^2 C}{\partial l^2} + \frac{\partial^2 C}{\partial m^2}\right) \quad (7)$$

where

$$U_l = \sqrt{(\overline{U_x} + u)^2 + (w)^2} \quad (8)$$

Since the concentration boundary layer is small compared with the viscous sublayer, the average velocity will vary linearly with y:

$$\overline{U_x} = \overline{S_x} y \quad (9)$$

where

$$\overline{S_x} = \frac{u^{*2}}{\nu} \quad (10)$$

The fluctuating components of the velocity u, v, and w may be expanded in a Taylor series in the vicinity of the wall. If these components are zero and the fluctuating shear stresses are not zero at the wall, then the leading term in the expansion of u and w will be of the order of y. When one makes use of the continuity equation, the leading term in the expansion of v must be of the order y^2 (2). Thus for very small values of y it may be assumed that

$$u = s_x y \quad (11)$$

$$w = s_z y \quad (12)$$

$$v = 0 \quad (13)$$

Combining Equations (8), (9), (11), and (12) one obtains

$$U_l = S_l y \quad (14)$$

where

$$S_l = \sqrt{(\overline{S_x} + s_x)^2 + (s_z)^2} \quad (15)$$

Equations (13) and (14) will be substituted into Equation (7) since the concentration boundary layer is very thin. Diffusion in the direction of flow is negligible by comparison with convection because of the small liquid diffusion coefficients and large Reynolds numbers. Equation (7) may now be simplified to

$$\frac{\partial C}{\partial t} + S_l y\frac{\partial C}{\partial l} = D\left(\frac{\partial^2 C}{\partial y^2} + \frac{\partial^2 C}{\partial m^2}\right) \quad (16)$$

For a square electrode $\frac{\partial^2 C}{\partial m^2} << \frac{\partial^2 C}{\partial y^2}$

if the width of the electrode is much larger than the thickness of the concentration boundary layer. The validity of such an assumption for a circular electrode is uncertain since the fluid flowing over the center line of the electrode will have a longer contact time than fluid flowing over the electrode near its edge. Thus the concentration gradient and second derivative in the m direction may be large. Nevertheless in order to obtain an analytical solution this term will be neglected. The justification for neglecting diffusion perpendicular to the flow will be found by comparing measured average mass transfer data with that which will be predicted from this analysis. The comparison is quite good if the circular electrode is considered as a rectangle whose effective length in the direction of flow is given by (*11*)

$$\frac{1}{(L_e)^{1/3}} = \frac{\int_0^{\Pi} \frac{1/2\, d_e^2 \sin^2\Psi}{(d_e \sin\Psi)^{1/3}} d\Psi}{\frac{\Pi d_e^2}{4}} \quad (17)$$

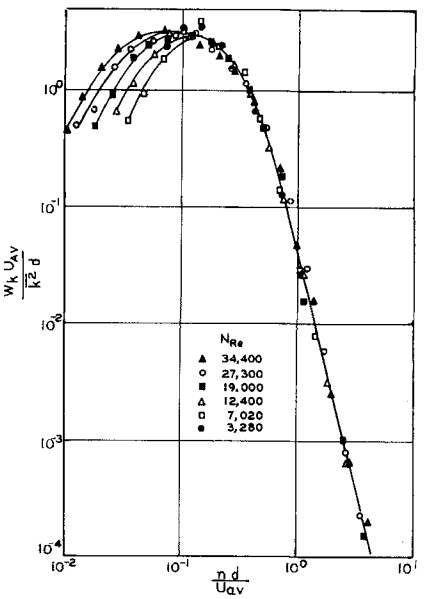

Fig 6. Mass transfer frequency spectra.

After the indicated integration this definition becomes

$$L_e = 0.820\, d_e \quad (18)$$

Equation (16) now may be written as

$$\frac{\partial C}{\partial t} + S_l\, y\frac{\partial C}{\partial l} = D\frac{\partial^2 C}{\partial y^2} \quad (19)$$

A first approximation to the solution of this equation may be made by neglecting the time variation of concentration which results in

$$S_l\, y\frac{\partial C}{\partial l} = D\frac{\partial^2 C}{\partial y^2} \quad (20)$$

with the boundary conditions

$$\begin{array}{lllll} (1) & l = 0 & y > 0 & C = C_B \\ (2) & l > 0 & y = 0 & C = C_w = 0 \\ (3) & l > 0 & y \to \infty & C = C_B \end{array} \quad (21)$$

The solution of this equation for the concentration profile is

$$\frac{C - C_w}{C_B - C_w} = \frac{\int_0^{\eta} e^{-\eta^3} d\eta}{\Gamma(4/3)} \quad (22)$$

where

$$\eta = \frac{y}{l^{1/3}}\left(\frac{S_l}{9D}\right)^{1/3} \quad (23)$$

A second approximation to the solution of Equation (19) may be made by integrating Equation (19) with respect to y and over the electrode surface and with the concentration profile from the first approximation to evaluate the integrals. Equation (19) may now be written as

$$\int_0^{L_e} dl \int_0^{\infty} \frac{\partial C}{\partial t} dy + \int_0^{L_e} dl \int_0^{\infty} y\, S_l \frac{\partial C}{\partial l} dy = \int_0^{L_e} dl \int_0^{\infty} D\frac{\partial^2 C}{\partial y^2} dy \quad (24)$$

The term on the right side of the equation is the total mass transfer rate over the whole electrode which may be put on a unit area basis by dividing the equation by the electrode area. This unit area mass transfer rate which is averaged over the electrode surface may be expressed as the mass transfer coefficient by dividing the equation by $C_B - C_W$. The resulting equation is

$$\frac{1}{L_e}\frac{\partial}{\partial t}\int_0^{L_e} dl \int_0^{\infty} \frac{C - C_B}{C_B - C_W} dy + \frac{1}{L_e}\int_0^{L_e} d\left\{\int_0^{\infty} \frac{y\, S_l\,(C - C_B)}{C_B - C_W} dy\right\} = -\frac{N}{C_B - C_W} = -K \quad (25)$$

The integrals are evaluated with the first approximation concentration profile expressed by Equation (22) with the definition of η (Equation 23). The result is

$$K = \frac{3}{2\,\Gamma(4/3)\,(9)^{1/3}}\left(\frac{D^2 S_l}{L_e}\right)^{1/3} + \frac{\phi\, 9^{1/3}\, 3}{4}(D L_e)^{1/3}\frac{\partial(S_l^{-1/3})}{\partial t} \quad (26)$$

where

$$\phi = \int_0^{\infty}\left[1 - \frac{\int_0^{\eta} e^{-\eta^3} d\eta}{\Gamma(4/3)}\right] d\eta = 0.505171 \quad (27)$$

This constant was evaluated with a numerical integration based on the values of

$$\int_0^{\eta} e^{-\eta^3} d\eta \quad (28)$$

tabulated by Abramowitz (*1*).

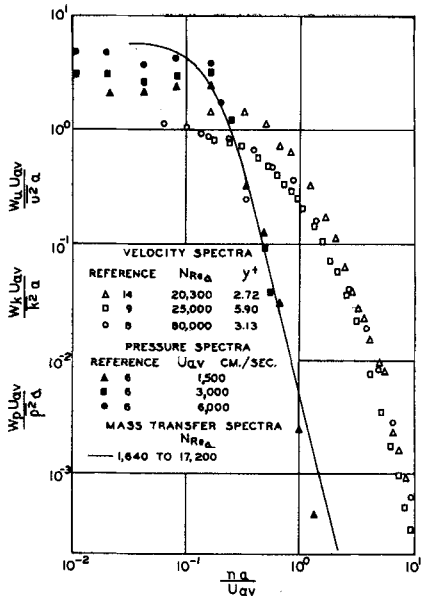

Fig. 7. Comparison of velocity, pressure, and mass transfer spectra.

The derivative may be evaluated with the relation for S_i from Equation (15):

$$\frac{\partial(S_i^{-1/3})}{\partial t} = -\frac{1}{3} S_i^{-7/3} \bar{S}_x \frac{\partial s_x}{\partial t} \tag{29}$$

where second-order terms in the s_x and s_z have been neglected. Equation (26) becomes

$$K S_i^{7/3} = \frac{3}{2\Gamma(4/3)(9)^{1/3}} \left(\frac{D^{2/3}}{L_e^{1/3}}\right) S_i^{8/3} - \frac{\phi L_e^{1/3} D^{1/3} 9^{1/3}}{4} \bar{S}_x \frac{\partial s_x}{\partial t} \tag{30}$$

The terms $S_i^{7/3}$ and $S_i^{8/3}$ may be expanded by using the binomial theorem and by neglecting second-order terms. Equation (30) may be rearranged to give

$$K = \frac{3}{2\Gamma(4/3)(9)^{1/3}} \left(\frac{D^2 \bar{S}_x}{L_e}\right)^{1/3} \left(1 + \frac{s_x}{3\bar{S}_x}\right) - \frac{\phi 9^{1/3}}{4} \left(\frac{L_e D}{\bar{S}_x}\right)^{1/3} \frac{\partial\left(\frac{s_x}{\bar{S}_x}\right)}{\partial t} \tag{31}$$

The time average of this equation is

$$\bar{K} = \frac{3}{2\Gamma(4/3)(9)^{1/3}} \left(\frac{D^2 \bar{S}_x}{L_e}\right)^{1/3} \tag{32}$$

Subtracting the time average equation from Equation (31) one gets the fluctuating mass transfer coefficient as a function of the fluctuating shear stress:

$$k = \frac{1}{2\Gamma(4/3)(9)^{1/3}} \left(\frac{D^2 \bar{S}_x}{L_e}\right)^{1/3} \left(\frac{s_x}{\bar{S}_x}\right) - \frac{\phi 9^{1/3}}{4} \left(\frac{L_e D}{\bar{S}_x}\right)^{1/3} \frac{\partial\left(\frac{s_x}{\bar{S}_x}\right)}{\partial t} \tag{33}$$

This equation is analogous to the form of the equation for a parallel R C electrical circuit where $s_x/\bar{S}_x$ is similar to the voltage and k is similar to the current. Consequently the term

$$\frac{1}{2\Gamma(4/3)(9)^{1/3}} \left(\frac{D^2 \bar{S}_x}{L_e}\right)^{1/3} \tag{34}$$

is similar to the reciprocal of the electrical resistance and is in effect the conductance of the concentration boundary layer. The term

$$\frac{\phi 9^{1/3}}{4} \left(\frac{L_e D}{\bar{S}_x}\right)^{1/3} \tag{35}$$

is similar to the electrical capacitance and could be termed the capacitance of the concentration boundary layer.

Equation (33) may be expressed in the following form by using the linear variation of average and by fluctuating velocity with distance from the wall [Equations (9) and (11)]:

$$3\frac{k}{\bar{K}} = \frac{u}{\bar{U}} - \tau \frac{\partial\left(\frac{u}{\bar{U}}\right)}{\partial t} \tag{36}$$

where

$$\tau = \frac{\phi \Gamma(4/3)(9)^{2/3}}{2} \left(\frac{L_e^2}{D \bar{S}_x^2}\right)^{1/3} \tag{37}$$

is the time constant of the concentration boundary layer.

It should be stressed that in addition to the assumptions outlined previously the validity of Equation (33) depends on the assumption $\partial C/\partial t$ being small compared with $S_i y(\partial C)/(\partial l)$, which was made in order to solve Equation (19). The following procedure was used to calculate the velocity intensity from the measurements of mass transfer intensity. The velocity fluctuation at any given frequency was assumed to be

$$\frac{u_n}{\bar{U}} = g \sin(2\Pi n t) \tag{38}$$

From Equation (36) the mass transfer fluctuation would be

$$3\frac{k_n}{\bar{K}} = g \sin(2\Pi n t) - \tau g 2\Pi n \cos(2\Pi n t) \tag{39}$$

Taking the mean square of both sides of the above equation one gets

$$9\frac{\overline{k_n^2}}{\bar{K}^2} = \frac{g^2}{2}[1 + (\tau 2\Pi n)^2] \tag{40}$$

The mean square of Equation (38) gives

$$\frac{\overline{u_n^2}}{\bar{U}^2} = \frac{g^2}{2} \tag{41}$$

Thus Equation (40) becomes

$$9\frac{\overline{k_n^2}}{\bar{K}^2} = \frac{\overline{u_n^2}}{\bar{U}^2}[1 + (\tau 2\Pi n)^2] \tag{42}$$

For a linear process the spectral density function therefore is

$$9\frac{W_k}{\bar{K}^2} = \frac{W_u}{\bar{U}^2}[1 + (\tau 2\Pi n)^2] \tag{43}$$

Rearranging and integrating one obtains

$$\frac{9}{\bar{K}^2}\int_0^\infty \frac{W_k}{1 + (\tau 2\Pi n)^2} dn = \int_0^\infty \frac{W_u}{\bar{U}^2} dn = \frac{\overline{u^2}}{\bar{U}^2} \tag{44}$$

By introducing the time scale d/U_{av} and taking the square root Equation (44) becomes

$$\frac{\sqrt{\overline{u^2}}}{\bar{U}} = 3\sigma \frac{\sqrt{\overline{k^2}}}{\bar{K}} \tag{45}$$

where

$$\sigma = \left[\int_0^\infty \frac{W_k U_{av}}{\overline{k^2} d} \left\{1 + 4\pi^2 \left(\frac{nd}{U_{av}}\right)^2 \left(\frac{U_{av}\tau}{d}\right)^2\right\}^{-1} d\left(\frac{nd}{U_{av}}\right)\right]^{1/2} \tag{46}$$

and the dimensionless time constant is given by

$$\frac{U_{av}\tau}{d} = 8.236 \left(\frac{L_e}{d}\right)^{2/3} (N_{Sc})^{1/3} (N_{Re})^{-1/6} \tag{47}$$

It is apparent from Equation (47) that the time constant can be made smaller by designing the experiment so that the electrode size and Schmidt number are smaller. For very small values of the time constant the capaci-

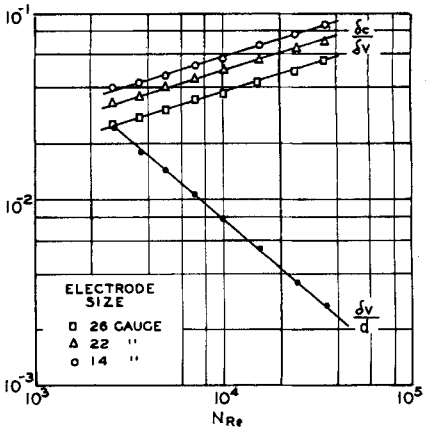

Fig. 8. Concentration boundary layer and viscous sublayer thickness.

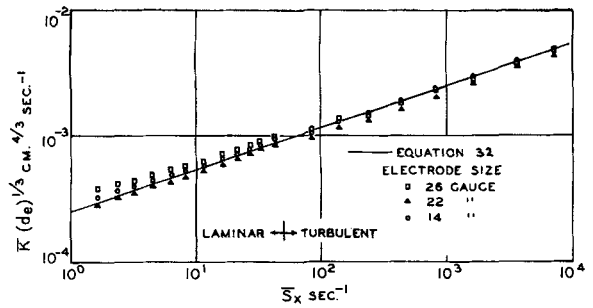

Fig. 9. Variation of average mass transfer coefficient with average wall shear stress.

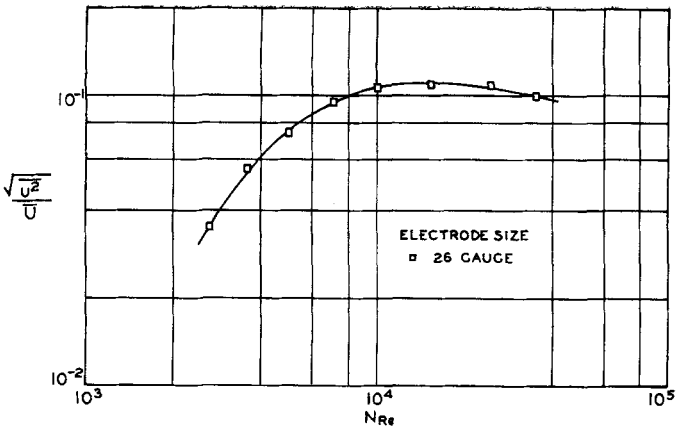

Fig. 10. Velocity intensities calculated from mass transfer measurements.

tance effect may be neglected, and the mass transfer fluctuations will be directly proportional to the velocity fluctuations.

A preliminary interpretation of the mass transfer measurements as velocity measurements will now be made, and the calculated velocity data will be compared with velocity data measured with hot wire anemometry. The average mass transfer coefficients are a direct measure of the average velocity gradient at the wall and may be compared with Equation (32) when plotted as

$$\overline{K}\,(d_e)^{1/3} \text{ vs. } \overline{S}_x$$

in Figure 9. Also included in this figure is the result predicted by Equation (32) with the expression for equivalent length [Equation (17)]. The diffusion coefficient was calculated from the measured viscosity with an empirical relation given by Eisenburg (5):

$$D = \frac{T}{\mu} 2.50 \times 10^{-10} \frac{\text{sq. cm. poise}}{\text{sec. °K.}} \quad (48)$$

Figure 9 shows that the generalized form of Equation (32)

$$\overline{K} = \epsilon(\overline{S}_x)^{\gamma} \quad (49)$$

is valid over a wide range of shear stress both in laminar and turbulent flow. The constant ϵ predicted by Equation (32) is in good agreement with the data from the 14 and 26 gauge electrodes except in the region of low shear stress corresponding to low Reynolds numbers in laminar flow. The disagreement of the data from the 22 gauge electrodes with the predicted value of ϵ is probably due to experimental error.

The value of 1/3 for γ predicted by Equation (32) is confirmed by the data from each sized electrode except at very low flow rates. The disagreement between measured and predicted coefficients at low flow rates could be due to the neglect of diffusion effects normal to the flow direction in the derivation of Equation (32). As a result average coefficients predicted by Equation (32) would be too low. This is the effect displayed for the low shear stress measurements. However for the turbulent region the average data support the use of 1/3 for the value of γ which also appears in the relation between mass transfer intensity and velocity intensity [Equation (45)].

It has been shown that the concentration boundary layer is less than one-tenth the viscous sublayer thickness for the experiments reported. Thus the region of the flow field which is influencing the mass transfer intensity measurements is $y^+ < 0.5$. The values of the velocity intensities calculated from mass transfer intensity measurements with Equation (45) and mass transfer spectra to evaluate σ are shown in Figure 10. They should be an indication of the limiting value of the intensity as the wall is approached.

Measurements of fluctuating velocities using hot wire anemometry have been made by Laufer (*10*) in a pipe, Laufer (*9*) in a two-dimensional channel, and Klebanoff (*8*) in a turbulent boundary layer over a flat plate.

The comparison between measured velocity intensities in the region of $y^+ < 15$ and the maximum velocity intensity in the region at $y^+ < 0.5$ predicted from mass transfer intensity measurements on 26 gauge electrodes is shown in Figure 11. The velocity data obtained with hot wire anemometry are subject to error owing to nonuniform flow over the wire length since no length corrections have been applied to velocity data. No velocity data are available in the region of $y^+ < 1$ owing to the difficulty of making measurements with probes very near the wall. It is difficult to ascertain from the hot wire measurements what the value of the limiting velocity intensity is as $y^+ \to 0$. However it appears the limiting velocity intensity calculated from mass transfer measurements is not in exact agreement with intercepts which could be extrapolated from hot wire measurements.

CONCLUSIONS

It may be concluded that a diffusion controlled electrolytic reaction on a circular electrode which is part of the pipe wall can be used to indicate the nature of the velocity field near a pipe wall. However for the present system two serious limitations prevented accurate direct quantitative interpretations of the mass transfer measurements as velocity measurements. The first limitation was due to the capacitance effect of the concentration boundary layer. Thus the velocity fluctuations were not directly proportional to the measured mass transfer fluctuations, the actual relationship being expressed as in Equation (36). It was found that the time constant τ could be decreased by decreasing the electrode size and Schmidt number.

The second limitation was that the flow over the electrode was nonuniform because the diameters of the electrodes were of the same order of magnitude as the integral scale of the circumferential correlation. This caused difficulties in interpreting the fluctuating quantities due to the averaging out of the effects of small, high frequency flow disturbances over the electrode surface. It was found that the errors due to nonuniform distribution of flow could be reduced when the effective electrode width was reduced.

In spite of these limitations the measurements reported in this paper support the following conclusions about the nature of the unsteady flow in the viscous region of turbulent pipe flow.

1. The local turbulent velocity intensities in the direction of flow calculated from mass transfer intensity measurements have values of at least 10% near the wall.

2. The time scale of the disturbances in the viscous sublayer is determined by the bulk parameters: averaged fluid velocity and characteristic length of the system, that is pipe radius, channel half-width, or boundary-layer thickness.

3. The longitudinal integral scale of the disturbances in the viscous sub-

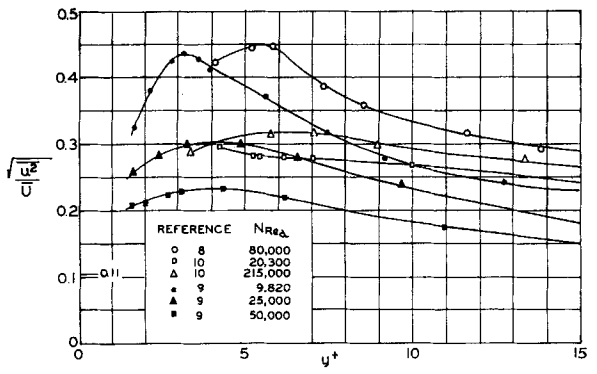

Fig. 11. Local turbulent velocity intensities.

layer is of the order of the pipe radius, while the circumferential integral scale is an order of magnitude smaller.

ACKNOWLEDGMENT

Fellowship support for one of the authors was received from Visking Corporation and Monsanto Chemical Company. Financial support was also received from National Science Foundation Grant G-14788.

NOTATION

A = electrode surface area, sq. cm.
a = characteristic length, pipe radius, channel half-width, boundary-layer displacement thickness, cm.
B = as subscript bulk
C = instantaneous concentration of ferricyanide, moles/liter
D = diffusion coefficient, sq. cm./sec.
d = pipe diameter—2.54 cm.
d_e = electrode diameter, cm.
g = amplitude in Equation (38)
K = instantaneous mass transfer coefficient, $K = \frac{N}{C_B - C_W}$, cm./sec.
$\overline{K}$ = average mass transfer coefficient, $\overline{K} = \lim_{\theta\to\infty} \frac{1}{\theta}\int_0^\theta K dt$, cm./sec.
k = fluctuating component of the mass transfer coefficient, $k = K - \overline{K}$, cm./sec.
L_e = equivalent weighted electrode length, Equation (17), cm.
l = instantaneous flow direction over electrode surface, cm.
m = direction normal to instantaneous flow direction, cm.
N = instantaneous unit area mass transfer rate of ferricyanide, moles/sec. sq. cm.
n = frequency, cycles/sec.
N_{Re} = Reynolds number based on pipe diameter and bulk average velocity
N_{Sc} = Schmidt number, ν/D
p = fluctuating component pressure, dynes/sq. cm.
R = correlation coefficient; R_l longitudinal; R_c circumferential, $R = \frac{k_1 k_2}{\sqrt{\overline{k_1^2}}\sqrt{\overline{k_2^2}}}$
S = instantaneous velocity gradient, sec.$^{-1}$
$\overline{S}$ = average velocity gradient, sec.$^{-1}$
s = fluctuating component of velocity gradient, sec.$^{-1}$
t = time, sec.
U = instantaneous velocity, cm./sec.
$\overline{U}$ = average velocity x direction; U_{av}, bulk averaged velocity, cm./sec.
u = fluctuating component of velocity x direction, cm./sec.
u^+ = dimensionless average velocity $\overline{U}/u^*$
u^* = friction velocity, cm./sec.
v = fluctuating component of velocity in y direction, cm./sec.
W = subscript wall
W_k = spectral density function of mean square fluctuating mass transfer coefficient, $\overline{k^2} = \int_0^\infty W_k dn$, sq. cm./sec.
W_u = spectral density function of mean square fluctuating velocity in x direction, $\overline{u^2} = \int_0^\infty W_u dn$, sq. cm./sec.
W_p = spectral density function of mean square fluctuating pressure, $\overline{p^2} = \int_0^\infty W_p dn$, sq. dynes-sec./cm.^{4}
w = fluctuating component of velocity in z direction, cm./sec.
x = coordinate parallel to pipe axis; center to center electrode spacing in x direction, cm.
y = coordinate perpendicular to pipe wall, cm.
y^+ = dimensionless distance from wall, yu^*/ν
z = coordinate parallel to pipe wall, perpendicular to average flow; center to center electrode spacing z direction, cm.

Greek Letters

Γ = gamma function; $\Gamma(4/3) = 0.8929795116$
γ = exponent in Equation (49)
δ_c = concentration boundary-layer thickness, Equation (5), cm.
δ_v = viscous sublayer thickness, Equation (6), cm.
ϵ = constant in Equation (49), cm./sec.$^{2/3}$
η = defined by Equation (23)
θ = period of time, sec.
Λ = integral scale; Λ_l longitudinal integral scale; Λ_c circumferential integral scale $\Lambda = \int_0^\infty R dx$, cm.
μ = viscosity, centipoise
ν = kinematic viscosity, sq. cm./sec.
ρ = density, g./cc.
σ = defined by Equation (46)
τ = time constant defined by Equation (37), sec.
ϕ = defined by Equation (27) = 0.505171
Ψ = angular direction on circular electrode

LITERATURE CITED

1. Abramowitz, M., *J. Math. Phys.*, **20**, 162 (1951).
2. Corrsin, S., "Some Current Problems in Turbulent Shear Flow," Chapt. 15, p. 393, Naval Hydrodynamics Publication 515, National Academy of Sciences, National Research Counsel (1957).
3. Delahay, P., "New Instrumental Methods in Electrochemistry," p. 217, Interscience, New York (1954).
4. Dryden, H. L., G. B. Schubauer, W. C. Mock, Jr., and H. K. Skramstad, *Natl. Advisory Comm. Aeronaut. Tech. Rept. 581* (1937).
5. Eisenburg, M., C. W. Tobias, and C. R. Wilke, *J. Electrochem. Soc.*, **103**, 413 (1956).
6. Harrison, M., "Pressure Fluctuations on the Wall Adjacent to a Turbulent Boundary Layer," David Taylor Model Basin Hydromechanics Laboratory Research and Development Report 1260 (1958).
7. Hinze, J. O., "Turbulence," p. 92, McGraw-Hill, New York (1959).
8. Klebanoff, P. S., *Natl. Advisory Comm. Aeronaut. Tech. Note 3187* (1954).
9. Laufer, J., *Natl. Advisory Comm. Aeronaut. Tech. Rept. 1053* (1951).
10. ———, *Natl. Advisory Comm. Aeronaut. Tech. Rept. 1174* (1954).
11. Reiss, L. P., M.S. thesis, University of Illinois, Urbana, Illinois (1960).
12. ———, Ph.D. thesis, University of Illinois, Urbana, Illinois (1962).
13. ———, and T. J. Hanratty, *A.I.Ch.E. Journal*, **8**, 245 (1962).
14. Sandborn, V. A., *Natl. Advisory Comm. Aeronaut. Tech. Note 3266* (1955).

Manuscript received June 22, 1962; revision received November 28, 1962; paper accepted December 3, 1962. Paper presented at A.I.Ch.E. Chicago meeting.